Journal of Sustainable Development of Smart Energy Networks

http://www.sdewes.org/jsdsen

Year 2026, Volume 1, Issue 3, 2030689

Original Research Article

Unlocking Energy Flexibility in Multi-Carrier Energy Hubs with Integrated Electrical-Thermal Demand Response

Amin Barati, Nicola Bianco, Marialaura Di Somma

[1]Department of Industrial Engineering, University of Naples Federico II, Naples, Italy

e-mail: amin.barati@unina.it, nicola.bianco@unina.it, marialaura.disomma@unina.it

Cite as: Barati, A., Bianco, N., Di Somma, M., Unlocking Energy Flexibility in Multi-Carrier Energy Hubs with Integrated Electrical-Thermal Demand Response, J. sustain. dev. smart. en. net., 1(3), 2030689, 2026,
DOI: https://doi.org/10.13044/j.sdsen.d3.0689

ABSTRACT

The global transition toward multi-energy systems positions energy hubs as the central architecture for coordinating electricity, heating, cooling, and hydrogen resources within a unified framework. This paper aims to optimize day-ahead scheduling for a smart energy hub, with emphasis on minimizing operational costs while accounting for environmental impacts. We develop a comprehensive multi-objective model that integrates multiple technologies, including combined heat and power, power-to-hydrogen-to-power system, and an integrated demand response program. The demand response program reduces operational costs by 3% relative to the strict baseline. Furthermore, without demand response, the system is more reliant on the grid, importing 391 kWh of electricity, whereas with demand response, the total import decreases to 364 kWh. The proposed demand response program functions as a capacity manager, enabling the system to conduct energy arbitrage in a planned manner by moving loads to the lowest-price windows and keeping other equipment operating efficiently.

KEYWORDS

Smart energy hub, Integrated demand response program, Power-to-hydrogen-to-power, Energy management, Energy flexibility.

INTRODUCTION

Decarbonizing local energy systems requires the large-scale integration of Variable Renewable Energy (VRE) sources, such as wind and solar. However, the inherent intermittency of these resources can challenge supply adequacy and compromise thermal comfort in building-dominated Smart Energy Hubs (SEHs) [1]. During peak heating demand, traditional grids often revert to fossil-fuel technologies, creating a structural mismatch between the renewable generation profile and the thermal load profile. Batteries and other electrochemical systems are well-suited to fast, power-intensive operations but are economically unappealing for multi-hour, daily, and, more so, seasonal energy shifting. This constraint underscores the significance of Power-to-X solutions, specifically Power-to-Hydrogen-to-Power (P2H2P), which offers a high-density, long-duration material that bridges the electrical and thermal domains and facilitates further VRE integration [2].

Nevertheless, hydrogen alone is insufficient to bridge the economic divide in existing fixed-price markets, where low-cost fossil fuels continue to dominate operational choices. This encourages the transition from a single-technology approach to an SEH, whereby electricity, heating, cooling and hydrogen resources are co-optimized as a system rather than operated independently. In an SEH, there must be an optimization-based approach that models both

unit-commitment decisions, energy conversions, and storage dynamics, and that transparently measures trade-offs between operating costs and environmental performance. In addition, the use of integrated thermal-electrical Demand Response Programs (DRPs) makes end users a flexible resource. It enables the SEH to manage loads over time, reduce upstream grid loads, and operate Combined Heat and Power (CHP) and hydrogen systems in accordance with their economic and efficiency targets. Here, the selected optimization framework is motivated by a single goal: to use system-level flexibility to enable high-renewable, low-carbon operation that is both technically and economically viable.

Recent studies have examined the role of energy conversion technologies and supervisory control strategies in SEHs. However, a considerable portion of this literature addresses only key performance dimensions, such as environmental impact, operational flexibility, and reliability. Several works analyze SEH energy management, but either omit DRPs or treat them in a simplified way, thereby limiting the SEH's ability to exploit demand-side flexibility [3]. In [4], the authors developed a robust optimization model that accounts for uncertainty for a single SEH, but thermal DRPs and their role in reducing operational costs were not considered. Similarly, other SEH formulations integrate natural gas and electricity networks with cloud-based demand-side management, while neglecting thermal DRPs, or develop Mixed Integer Linear Programming (MILP) models with detailed Power-to-X representations but without explicit flexibility analysis or DRP modeling [5]. In [6], a MILP optimization model was established for SEH analysis, along with an open-source power-to-x model that incorporates variable electrolyzer efficiency; however, flexibility analysis and DRPs were overlooked. Authors in [7] utilized a computational model-based approach to optimize SEHs to minimize total operational costs while ensuring reliability and efficiency; however, they overlooked thermal DRP and focused solely on electrical DRPs.

On the other hand, although several studies have modelled DRPs and storage systems in SEHs, the hydrogen system is often omitted from the optimization framework [8]. Bi-level SEH optimization has been proposed in [9] to coordinate energy-carbon flows and incorporates low-carbon DRP, yet they exclude P2H2P systems and therefore cannot quantify the contribution of sector-coupling through the hydrogen system. Another study in [10] adopted mixed-integer nonlinear programming to optimize SEH under DRPs, but omitted hydrogen technologies such as electrolyzers and fuel cells for VRE management. Techno-economic assessments of SEHs with DRPs and energy storage sometimes use Monte Carlo methods to account for uncertainty, while still excluding the hydrogen chain as a flexibility option [11]. Authors in [12] employed a robust SEH operation that manages uncertainties using compressed-air storage and Electric-vehicle-based load response, while overlooking the role of P2H2P systems in SEH operation. Additional studies employ robust operation strategies using compressed-air storage or electric-vehicle-based load response, or design multi-timescale scheduling for SEH with DRPs, but still do not include hydrogen storage or fuel cells in the system model [13].

From an optimization standpoint, sustainable SEH operation typically requires balancing multiple objectives, most notably operating cost and environmental performance. Multi-objective optimization techniques, such as normalized weighted sum methods, have been successfully employed to obtain cost-emission trade-offs in SEH and related applications [14], [15]. Nevertheless, several SEH studies still adopt single-objective formulations. For instance, stochastic programming has been applied to SEH energy management, with parameter uncertainty treated using two-point estimate methods; however, only the total operating cost is minimized, and other essential objectives, such as emissions or flexibility metrics, are not explicitly considered [16]. Authors in [17] suggested a multi-time-scale technique for optimizing an SEH that accounts for various energy storage components and their respective prices as a single-objective problem.

In addition to the above, several recent studies have further advanced SEH modelling by integrating P2H2P and enhanced demand-side management. Eco-environmental stochastic

scheduling frameworks and hydrogen-based SEH with integrated DRP have been proposed, but DRPs are predominantly modelled on the electrical side, and thermal flexibility remains underexploited [18], [19]. Multi-objective formulations for socio-economic SEHs and virtual energy hubs quantify cost-emission satisfaction trade-offs, yet they typically omit a complete P2H2P within a unified single SEH operational framework [20], [21]. Furthermore, recent reviews on hydrogen integration in multi-energy systems underline the strategic role of P2H2P for long-duration flexibility and sector coupling, while calling for operational models that explicitly capture its interaction with demand response inside hub architectures [22].

In summary, prior research has advanced SEH modelling through robust, stochastic, and multi-objective formulations and has separately explored DRP and hydrogen-based storage as flexibility options. Yet, there is still no comprehensive framework that simultaneously models a single SEH with CHP, hydrogen production and storage, and integrated thermal-electrical DRPs, while jointly optimizing economic and environmental objectives. Building on these gaps, the present work develops a multi-objective MILP model that quantifies the economic value of internal flexibility, assesses its impact on grid reliance and emissions, and provides a transparent basis for integrating P2H2P and DRPs into future SEH configurations.

In this study, a comprehensive SEH is formulated for day-ahead optimization, in which operational costs and CO_2 emissions are simultaneously minimized within a multi-objective framework. The SEH explicitly incorporates a complete hydrogen subsystem (electrolyzer, storage, and fuel cell) together with integrated thermal and electrical DRPs as internal flexibility resources.

The main novelties and contributions of this work are summarized as follows:

- A detailed multi-objective MILP model is developed for an SEH that couples electricity, heating, cooling, and hydrogen flows, enabling the joint assessment of economic and environmental performance.
- Integrated thermal and electrical DRPs are explicitly modelled and integrated into the SEH scheduling problem, so that demand-side flexibility can be co-optimized with energy storage and conversion assets.

The suggested structure can be subjected to policy analysis and investment planning because, under various market and technical conditions, it explicates the economic worth of flexibility. The findings further reveal the potential of integrating operational optimization with market-driven demand-side strategies to enhance resilience and reduce costs in distributed energy systems.

This work is organized as follows. In Section 2, the mathematical formulation of the optimization problem is presented. It also provides a brief introduction to the methodology that underpins our study and multi-objective optimization. The case study is presented in Section 3. In this paper, we compare the performance of the optimization model with DRP and non-DRP environments. In addition, we examine how DRPs affect operational scheduling. In Section 4, we wrap up the paper by reviewing our key findings, discussing their implications for SEH optimization, and suggesting directions for future research.

MATHEMATICAL FORMULATION OF THE SEH

This section delineates the mathematical model of the proposed SEH. The primary principle of the utilized SEH is illustrated in **Figure 1**. The proposed system includes various energy technologies, such as a CHP system, a gas-fired boiler, VRE, a transformer unit, a hydrogen-based system, electrical, thermal, and cooling energy storage, an absorption chiller, an electric chiller, and electrical and thermal DRPs.

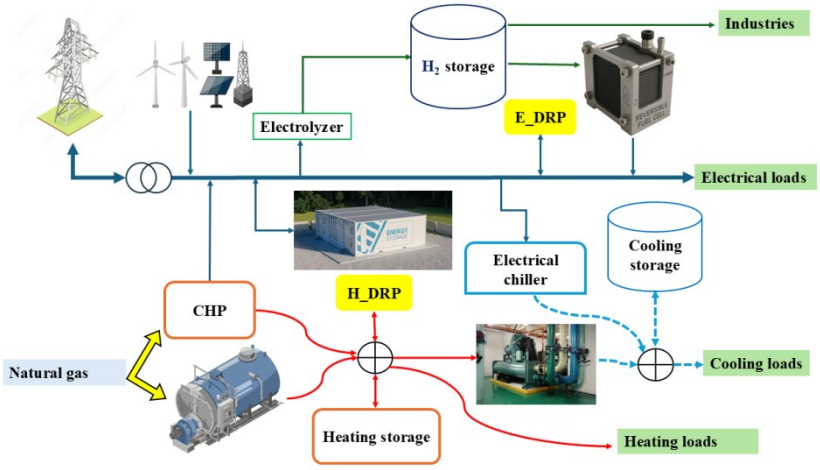

Figure 1. The proposed SEH architecture

Figure 2 illustrates the workflow for the optimal operation of the proposed SEH. The process starts with model formation, where the SEH architecture is specified and the mathematical models of all conversion, storage, and demand-side units are established, followed by the collection of demand profiles, price signals, VRE generation, and emission factors as input data. These inputs feed the optimization block, which is formulated as a multi-objective MILP that enforces device constraints, storage dynamics, and explicit modelling of thermal-electrical demand flexibility, ensuring a transparent and reproducible scheduling framework. Case Study I then provides a reference operation by optimizing the SEH without demand-side management, whereas Case Study II activates both thermal and electrical DRPs to exploit internal flexibility. Finally, the results of two case studies are compared and analyzed, with an exploration of the role of DRPs in system eco-environmental aspects, and key findings and contributions are summarized.

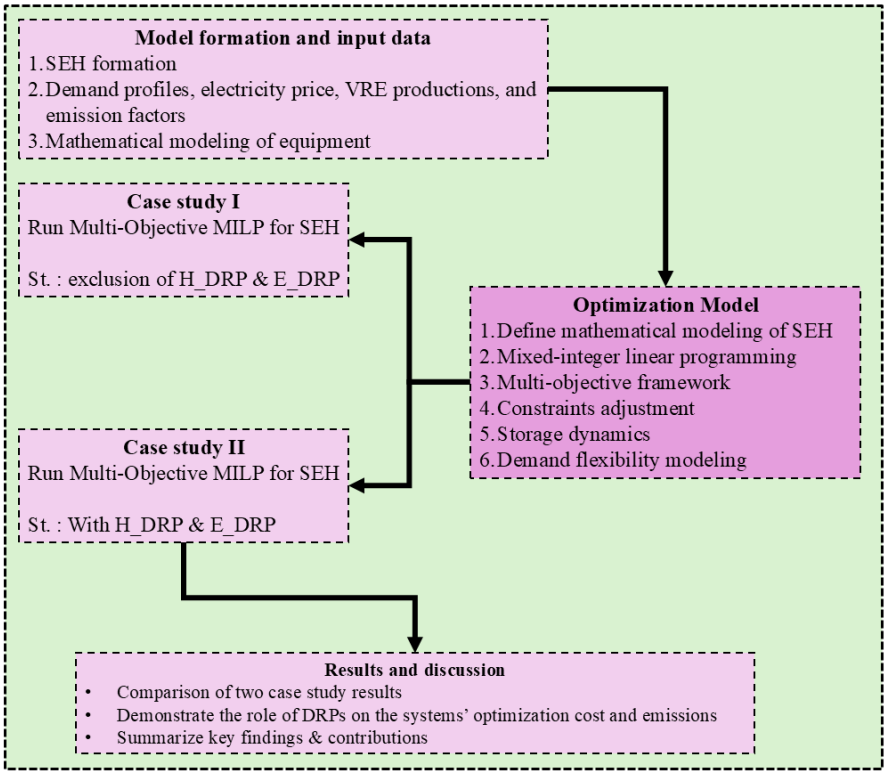

Figure 2. The entire workflow of SEH optimization

The Operational Cost Function

Eq. (1) presents the multi-objective function that integrates the cost function and system emissions. Eq. (2) also illustrates the cost function for the entire system, including costs for electricity procured from the upstream grid, operational and maintenance costs of the CHP and boiler, gas consumption costs for gas-fired units, and costs associated with load curtailment. Concurrently, Eq. (3) is used to simulate emissions from grid- and gas-fired equipment, including boilers and CHP systems.

$$\text{minimize } Z_{\mathrm{f}} = W_1 \times \left({Z_1}/{\left(Z_1^{\max} - Z_1^{\min}\right)} \right) + W_2 \times \left({Z_2}/{\left(Z_2^{\max} - Z_2^{\min}\right)} \right) \tag{1}$$

$$Z_1 = \sum_t \{P_{\mathrm{g}}^t \times \gamma_t + G_{\mathrm{chp}}^t \times \lambda_t + \left(PE_{\mathrm{chp}}^t + PH_{\mathrm{chp}}^t\right) \times OM_{\mathrm{CHP}} + (G_{\mathrm{b}}^t \times \lambda_t) + (PH_{\mathrm{b}}^t \times OMb) + (P_{\mathrm{curt}}^t \times PEN_{\mathrm{curt}})\} \tag{2}$$

$$\mathrm{Z}_2 = \sum_t (P_{\mathrm{g}}^t \times CI_{\mathrm{G}}) + (G_{\mathrm{chp}}^t + G_{\mathrm{b}}^t) \times CI_{\mathrm{gas}} \times LHV \tag{3}$$

Energy Storage

Improvement of the system's economic and reliability indices be achieved by using energy storage devices that store energy during low-cost periods and discharge it when required. This study employs electrical and thermal storage systems. For comprehension of electrical energy storage systems, the subsequent equations are applicable:

$$E_{\mathrm{es}}^{t+1} = E_{\mathrm{es}}^t(1 - \delta_{\mathrm{es}}) + P_{\mathrm{es,c}}^t \times \eta_{\mathrm{es,c}} \times \Delta t - \left({P_{\mathrm{es,d}}^t \times \Delta t}/{\eta_{\mathrm{es,d}}} \right) \forall t \tag{4}$$

$$E_{\mathrm{es}}^{\min} \leq E_{\mathrm{es}}^t \leq E_{\mathrm{es}}^{\max} \forall t \tag{5}$$

$$0 \leq P_{\mathrm{es,c}}^t \leq P_{\mathrm{es,c}}^{\max} \times K_{\mathrm{c}}^{\mathrm{e},t} \forall t \tag{6}$$

$$0 \leq P_{\mathrm{es,d}}^t \leq P_{\mathrm{es,d}}^{\max} \times K_{\mathrm{d}}^{\mathrm{e},t} \forall t \tag{7}$$

$$0 \leq K_{\mathrm{c}}^{\mathrm{e},t} + K_{\mathrm{d}}^{\mathrm{e},t} \leq 1 \forall t \tag{8}$$

$$E_{\mathrm{es}}^0 = E_{\mathrm{es}}^{24} \tag{9}$$

The energy balance of the electrical storage is presented in eq. (4). Technical constraints impose limitations on E_{es}^t, $P_{\mathrm{es,c}}^t$ and $P_{\mathrm{es,d}}^t$ as delineated in eq. (5) to eq. (7). Eq. (8) forbids concurrent charging and discharging of the energy storage system. Eq. (9) indicates that the energy stored must be constant at the first and last hour of the representative day.

To simulate the cooling storage, the following equations are provided:

$$E_{\mathrm{cs}}^{t+1} = E_{\mathrm{cs}}^t(1 - \delta_{\mathrm{cs}}) + P_{\mathrm{cs,c}}^t \times \eta_{\mathrm{cs,c}} \times \Delta t - \left({P_{\mathrm{cs,d}}^t \times \Delta t}/{\eta_{\mathrm{cs,d}}} \right) \forall t \tag{10}$$

$$E_{\mathrm{cs}}^{\min} \leq E_{\mathrm{cs}}^t \leq E_{\mathrm{cs}}^{\max} \forall t \tag{11}$$

$$0 \leq P_{\mathrm{cs,c}}^t \leq P_{\mathrm{cs,c}}^{\max} \times K_{\mathrm{c}}^{\mathrm{c},t} \forall t \tag{12}$$

$$0 \le P_{\mathrm{cs,d}}^{t} \le P_{\mathrm{cs,d}}^{\max} \times K_{\mathrm{d}}^{\mathrm{c},t} \; \forall t \tag{13}$$

$$0 \le K_{\mathrm{c}}^{\mathrm{c},t} + K_{\mathrm{d}}^{\mathrm{c},t} \le 1 \; \forall t \tag{14}$$

$$E_{\mathrm{cs}}^{0} = E_{\mathrm{cs}}^{24} \tag{15}$$

The modelling of the heating storage system is outlined as follows:

$$E_{\mathrm{hs}}^{t+1} = E_{\mathrm{hs}}^{t}(1-\delta_{\mathrm{hs}}) + P_{\mathrm{hs,c}}^{t} \times \eta_{\mathrm{hs,c}} \times \Delta t - \left(P_{\mathrm{hs,d}}^{t} \times \Delta t \Big/ \eta_{\mathrm{hs,d}} \right) \forall t \tag{16}$$

$$E_{\mathrm{hs}}^{\min} \le E_{\mathrm{hs}}^{t} \le E_{\mathrm{hs}}^{\max} \forall t \tag{17}$$

$$0 \le P_{\mathrm{hs,c}}^{t} \le P_{\mathrm{hs,c}}^{\max} \times K_{\mathrm{c}}^{\mathrm{h},t} \; \forall t \tag{18}$$

$$0 \le P_{\mathrm{hs,d}}^{t} \le P_{\mathrm{hs,d}}^{\max} \times K_{\mathrm{d}}^{\mathrm{h},t} \; \forall t \tag{19}$$

$$0 \le K_{\mathrm{c}}^{\mathrm{h},t} + K_{\mathrm{d}}^{\mathrm{h},t} \le 1 \; \forall t \tag{20}$$

$$E_{\mathrm{hs}}^{0} = E_{\mathrm{hs}}^{24} \tag{21}$$

Energy Balance of the SEH

The different energy balances of SEH are as follows:

$$\begin{aligned} P_{\mathrm{g}}^{t} + P_{\mathrm{pv}}^{t} + P_{\mathrm{wt}}^{t} + PE_{\mathrm{chp}}^{t} + P_{\mathrm{es,d}}^{t} + P_{\mathrm{down}}^{\mathrm{e},t} + P_{\mathrm{curt}}^{t} + P_{\mathrm{fc}}^{t} \\ = P^{\mathrm{el},t} + P_{\mathrm{es,c}}^{t} + P_{\mathrm{up}}^{\mathrm{e},t} + P_{\mathrm{elz}}^{t} + P_{\mathrm{ec}}^{t} \; \forall t \end{aligned} \tag{22}$$

$$-P_{\mathrm{g}}^{\max} \le P_{\mathrm{g}}^{t} \le P_{\mathrm{g}}^{\max} \; \forall t \tag{23}$$

$$PH_{\mathrm{chp}}^{t} + PH_{\mathrm{b}}^{t} + P_{\mathrm{hs,d}}^{t} + P_{\mathrm{down}}^{\mathrm{h},t} = P^{\mathrm{hl},t} + P_{\mathrm{hs,c}}^{t} + P_{\mathrm{up}}^{\mathrm{h},t} + PH_{\mathrm{ac}}^{t} \; \forall t \tag{24}$$

$$0 \le PH_{\mathrm{chp}}^{t} + PH_{\mathrm{b}}^{t} + P_{\mathrm{hs,d}}^{t} - P_{\mathrm{hs,c}}^{t} \le P_{\mathrm{h}}^{\max} \; \forall t \tag{25}$$

$$PH_{\mathrm{b}}^{t} = G_{\mathrm{b}}^{t} \times LHV \times \eta_{\mathrm{B}}^{\mathrm{h}} \tag{26}$$

$$0 \le G_{\mathrm{b}}^{t} \le G_{\mathrm{b}}^{\max} \tag{27}$$

$$PE_{\mathrm{chp}}^{t} = G_{\mathrm{chp}}^{t} \times LHV \times \eta_{\mathrm{chp}}^{\mathrm{e}} \tag{28}$$

$$PH_{\mathrm{chp}}^{t} = PE_{\mathrm{chp}}^{t} \times (\eta_{\mathrm{chp}}^{\mathrm{h}} / \eta_{\mathrm{chp}}^{\mathrm{e}}) \tag{29}$$

$$0 \le G_{\mathrm{chp}}^{t} \le G_{\mathrm{chp}}^{\max} \tag{30}$$

Eq. (22) maintains the active power balance constant. This means that the total power from the grid, renewable sources such as wind and solar, CHP output, storage discharge, and DRP adjustments equals the total power required for load consumption, storage charging, electrolysis, and electric chiller demand. The tie-line capacity limits in eq. (23) specify the maximum power that can be sent to and received from the utility grid. Eq. (24) does the same: it keeps the heating network in energy balance by balancing the heating rates from the CHP and

the boiler with the thermal load, the absorption chiller demand, and the storage discharge. The limits on the heat transmission network in eq. (25) further reduce the total heat rate output. The gas-fired technologies work as shown by eq. (26) to eq. (30). Finally, eq. (28) to eq. (30) show the modelling of the CHP unit.

As for the cooling section, the mathematical equations of both electrical and absorption chillers are as follows:

$$C_{\mathrm{ec}}^{t} + C_{\mathrm{ac}}^{t} + P_{\mathrm{cs,d}}^{t} = CL^{t} \ \forall t \tag{31}$$

$$C_{\mathrm{ac}}^{t} = \ PH_{\mathrm{ac}}^{t} \times COP_{\mathrm{ac}} \ \forall t \tag{32}$$

$$0 \leq PH_{\mathrm{ac}}^{t} \leq PH_{\mathrm{ac}}^{\max} \ \forall t \tag{33}$$

$$C_{\mathrm{ec}}^{t} = \ P_{\mathrm{ec}}^{t} \times COP_{\mathrm{ec}} \ \forall t \tag{34}$$

$$0 \leq P_{\mathrm{ec}}^{t} \leq P_{\mathrm{ec}}^{\max} \ \forall t \tag{35}$$

Eq. (31) represents the energy balance for the SEH in the cooling segment. Eq. (32) to eq. (35) show the modelling of absorption and electric chillers.

Hydrogen Model

The dynamics of the hydrogen loop are represented in eq. (36) to eq. (44). Eq. (36) and eq. (37) define the constraints of the Power-to-Gas process and establish the electrolyzer's allowable operating range. In contrast, eq. (38) and eq. (39) govern the Gas-to-Power re-electrification process via the fuel cell [23]:

$$P_{\mathrm{elz}}^{t} \leq P_{\mathrm{elz}}^{\max} \times I_{\mathrm{elz}}^{t} \tag{36}$$

$$P_{\mathrm{elz}}^{t} \geq P_{\mathrm{elz}}^{\min} \times I_{\mathrm{elz}}^{t} \tag{37}$$

$$P_{\mathrm{FC}}^{t} \leq P_{\mathrm{FC}}^{\max} \times I_{\mathrm{FC}}^{t} \tag{38}$$

$$P_{\mathrm{FC}}^{t} \geq P_{\mathrm{FC}}^{\min} \times I_{\mathrm{FC}}^{t} \tag{39}$$

Additionally, a binary logic constraint, as expressed in eq. (40), is implemented to prevent the concurrent operation of both units. The central inventory balance of the hydrogen tank is presented in eq. (41). This constraint is essential as it equilibrates internal energy arbitrage with external hydrogen demand $H_{2_{\mathrm{industry}}}^{t}$, thereby integrating the hub's storage function with its role as a fuel supplier. Eq. (43) and eq. (44) define the storage limits, whereas eq. (42) ensures a sustainable daily operational cycle:

$$0 \leq I_{\mathrm{FC}}^{t} + I_{\mathrm{elz}}^{t} \leq 1 \tag{40}$$

$$C_{\mathrm{H2}}^{t} = C_{\mathrm{H2}}^{t-1} + \eta^{\mathrm{elz}} \times P_{\mathrm{elz}}^{t} \times \Delta t - \left({P_{\mathrm{FC}}^{t} \times \Delta t} \Big/ {\eta^{\mathrm{FC}}} \right) - H_{2_{\mathrm{industry}}}^{t} \ \forall t \tag{41}$$

$$C_{\mathrm{H2}}^{0} = C_{\mathrm{H2}}^{24} \tag{42}$$

$$C_{\mathrm{H2}}^{0} \leq C_{\mathrm{H2}}^{\max} \tag{43}$$

$$C_{\mathrm{H2}}^{0} \geq C_{\mathrm{H2}}^{\min} \tag{44}$$

Demand Flexibility Models

Eq. (45) to eq. (49) show the flexibility of DRP. The main idea behind temporal load shifting is that the daily sum of load increments must equal the sum of load decrements, keeping the consumer's total energy demand constant. Eq. (46) and eq. (47) set the limits on the adjustable power based on participation factors. This is the flexible capacity available for this shift. Eq. (48) is a logical limit that prevents the system from operating in both "Load Up" and "Load Down" modes simultaneously. The model also lets users choose whether or not to shed load (curtailment) to keep the system balanced during critical peaks, as long as they stay within the upper limit in eq. (49):

$$\sum_{t} P_{\text{up}}^{\text{e},t} = \sum_{t} P_{\text{down}}^{\text{e},t} \tag{45}$$

$$0 \le P_{\text{up}}^{\text{e},t} \le MR_{\text{up}}^{\text{e}} P^{\text{el},t} \times I_{\text{up}}^{\text{e},t} \; \forall t \tag{46}$$

$$0 \le P_{\text{down}}^{\text{e},t} \le MR_{\text{down}}^{\text{e}} \times P^{\text{el},t} \times I_{\text{down}}^{\text{e},t} \; \forall t \tag{47}$$

$$0 \le I_{\text{up}}^{\text{e},t} + I_{\text{down}}^{\text{e},t} \le 1 \; \forall t \tag{48}$$

$$0 \le P_{\text{curt}}^{t} \le P^{\text{el},t} \times CO_{\text{curt}} \; \forall t \tag{49}$$

For thermal DRP, eq. (50) shows that the sum of the increases and decreases in the DRPs is zero. The maximum/minimum limitation for thermal load shifting is specified in eq. (51) to eq. (52), whilst the prevention of simultaneous load shifting is discussed in eq. (53):

$$\sum_{t} P_{\text{up}}^{\text{h},t} = \sum_{t} P_{\text{down}}^{\text{h},t} \tag{50}$$

$$0 \le P_{\text{up}}^{\text{h},t} \le MR_{\text{up}}^{\text{h}} \times P^{\text{hl},t} \times I_{\text{up}}^{\text{h},t} \; \forall t \tag{51}$$

$$0 \le P_{\text{down}}^{\text{h},t} \le MR_{\text{down}}^{\text{h}} \times P^{\text{hl},t} \times I_{\text{down}}^{\text{h},t} \; \forall t \tag{52}$$

$$0 \le I_{\text{up}}^{\text{h},t} + I_{\text{down}}^{\text{h},t} \le 1 \; \forall t \tag{53}$$

Non-intrusive constraints. To ensure that the DRP remains non-intrusive within a residential context, the model implements several preserving constraints. In detail, eq. (45) and eq. (50) dictate that the daily sum of load increments must equal the sum of load decrements, ensuring the total energy demand of the consumer remains constant. The flexibility is bounded by participation factors ($MR_{\text{up}}^{\text{e}}$, $MR_{\text{down}}^{\text{e}}$, $MR_{\text{up}}^{\text{h}}$, and $MR_{\text{down}}^{\text{h}}$), which limit the shiftable load to a conservative fraction of the baseline demand, preventing significant disruptions to daily activities. Also, logical limits in eq. (48) and eq. (53) prevent the system from operating in 'Load Up' and 'Load Down' modes simultaneously, ensuring a stable and predictable load profile for the residents.

Multi-objective Framework

Multi-objective optimization involves problems characterized by multiple, often conflicting objectives. This is prevalent in energy systems, where one must evaluate economic and environmental factors concurrently. The weighted sum method is a direct and effective strategy for tackling such situations [24]. It assigns a weight to each objective and integrates them into a single objective. The decision-maker uses these weights to signify the relative significance of

each objective. It is possible to analyze trade-offs among objectives by adjusting the weights. This facilitates identifying a set of Pareto-optimal solutions that reflect the system's overall performance. The weighted-sum method remains a prevalent approach for optimizing multi-energy systems due to its simplicity and adaptability and is formulated in eq. (54):

$$f(x) = \min \sum_{i=1}^{m} w_i \times f_i(x), f_i(x), i = (1,2,3,\dots,m) \quad (54)$$

Several weighted coefficients w_i can be used, such that $\sum_{i=1}^{m} w_i = 1$, with $w_i \geq 0, i = (1,2,3,\dots,m)$. The SEH operator assigns weights to each objective function based on its intrinsic understanding of the situation. Objective normalization is essential to achieve a Pareto-optimal solution that is consistent with the decision-makers' weights, since objective functions may differ in magnitude. Therefore, to ascertain the weights, we employ eq. (55) to eq. (57):

$$U_i = w_i \times \theta_i \quad (55)$$

$$\theta_i = 1 \Big/ \left(f_i^{\max}(x) - f_i^{\min}(x)\right) \quad (56)$$

$$F(x) = U_i \times f_i(x) \quad (57)$$

where θ_i is the normalization factor [25].

CASE STUDIES AND SIMULATION RESULTS

Input Data

The paper examines a residential SEH comprising a cluster of six buildings, each with 20 apartments, on a winter day in Torino, Italy. The mathematical model was developed as an MILP, and the CPLEX solver was used to solve it. The geographic circumstances result in generally low wind speeds, rendering wind power economically unviable and nearly non-existent. Thus, this study excludes wind generation. The photovoltaic generation data for Turin is sourced from the Photovoltaic Geographical Information System website [26], as illustrated in **Figure 3**, whereas the thermal and electrical storage parameters are provided in **Table 1**.

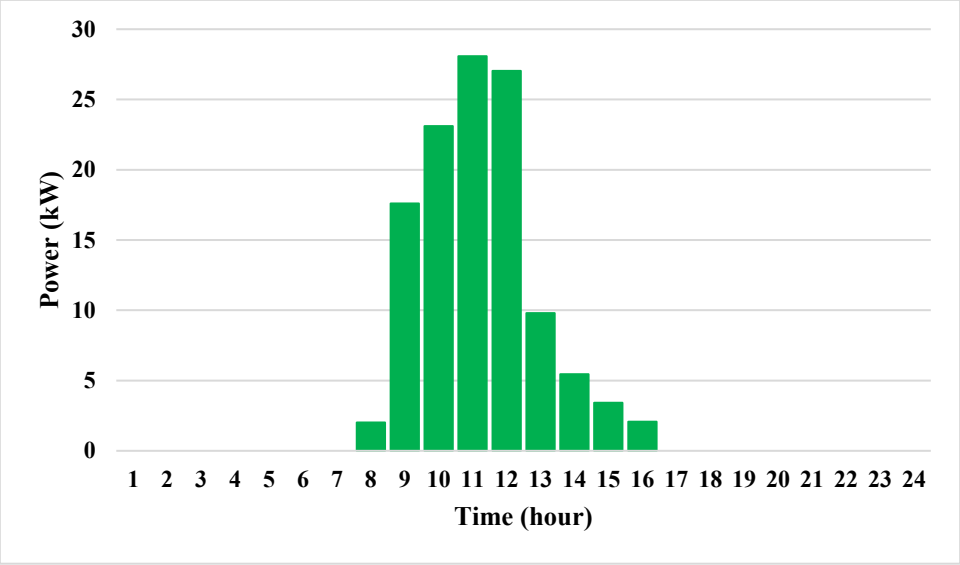

Figure 3. The PV generation profile for Torino on a winter day [26]

Table 1. Data for electrical and thermal storage systems [2]

	SEH
$E_{\text{es}}^{\max}$ [kWh]	100
$E_{\text{es}}^{\min}$ [kWh]	10
$P_{\text{es,c}}^{\max}$ [kWh]	20
$P_{\text{es,d}}^{\max}$ [kWh]	20
$E_{\text{hs}}^{\max}$ [kWh]	160
$E_{\text{hs}}^{\min}$[kWh]	30
$P_{\text{hs,c}}^{\max}$ [kWh]	40
$P_{\text{hs,d}}^{\max}$ [kWh]	40
δ_{es}	0.02
δ_{hs}	0.02
$\eta_{\text{es,c}}$	0.9
$\eta_{\text{es,d}}$	0.9
$\eta_{\text{hs,c}}$	0.9
$\eta_{\text{hs,d}}$	0.9

The parameters of the PV system, CHP, Boiler, and DRPs are shown in **Table 2**.

Table 2. Parameters of PV, Boiler, CHP unit, and DRPs

$\boldsymbol{OM}_{\text{CHP}}$ [$^{\text{cEUR}}/_{\text{kWh}}$]	2	$\boldsymbol{\eta}_{\text{CHP}}^{\text{e}}$	0.35
$\boldsymbol{OM}_{\text{B}}$ [$^{\text{cEUR}}/_{\text{kWh}}$]	2.7	$\eta_{\text{CHP}}^{\text{h}}$	0.48
$\boldsymbol{MR}_{\text{up}}^{\text{e}}$ [kW]	0.5	η_{B}	0.9
$\boldsymbol{MR}_{\text{up}}^{\text{e}}$ [kW]	0.2	COP_{ec}	4
$\boldsymbol{MR}_{\text{up}}^{\text{e}}$ [kW]	0.5	PEN_{curt}[$^{\text{cEUR}}/_{\text{kWh}}$]	80
$\boldsymbol{MR}_{\text{up}}^{\text{e}}$ [kW]	0.2	COP_{ac}	1.2
$\boldsymbol{\delta}_{\text{pv}}$	0.14	Co_{curt}	0.25
$\boldsymbol{MR}_{\text{up}}^{\text{e}}$ [kW]	300	CI_{g} [$\frac{\text{kg}}{\text{kWh}}$]	0.354
$\boldsymbol{MR}_{\text{up}}^{\text{e}}$ [kW]	200	CI_{gas} [$\frac{\text{kg}}{\text{kWh}}$]	0.202

The input data for the cooling section is presented in **Table 3 [2]**.

Table 3. Data on cooling storage and chillers

	SEH
$\boldsymbol{E}_{\text{cs}}^{\max}$ [kWh]	300
$\boldsymbol{E}_{\text{cs}}^{\min}$ [kWh]	60
$\boldsymbol{P}_{\text{cs,c}}^{\max}$ [kW]	120

$P_{cs,d}^{max}$ [kW]	140
PH_{ac}^{max} [kW]	180
$P_{cooling}^{max}$ [kW]	50
P_{ec}^{max} [kW]	80
$\eta_{cs,c}$	0.97
$\eta_{cs,d}$	0.95
δ_{cs}	0.02

The daily electricity price is obtained from the Transparency Platform (entsoe) [27], as depicted in Figure 4.

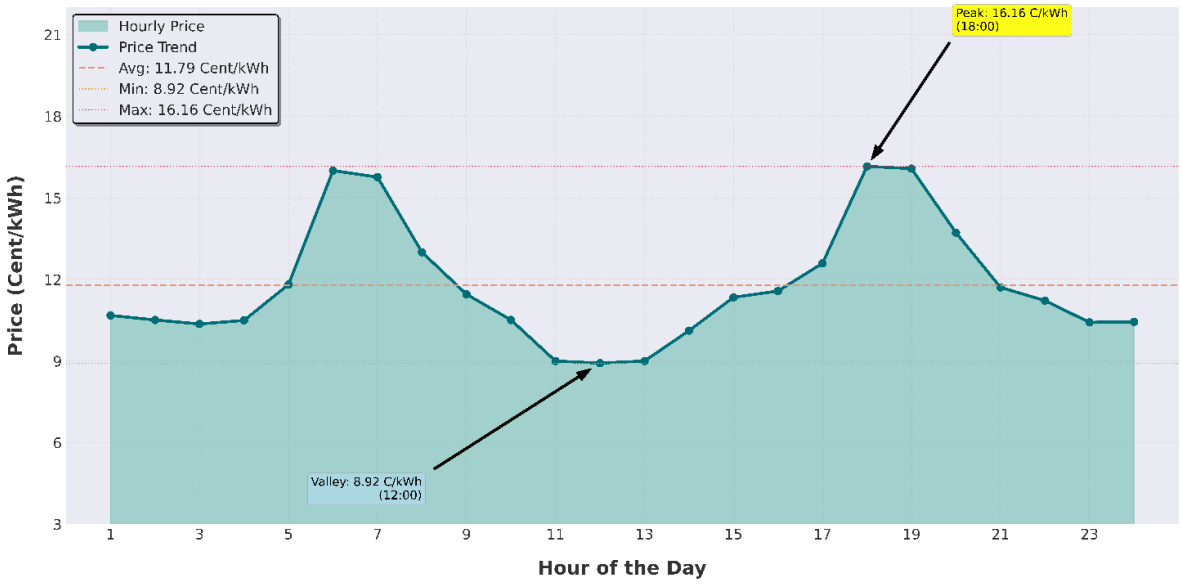

Figure 4. The day-ahead electricity price [27]

The load profiles of the residential building cluster are illustrated in Figure 5 [28], [29].

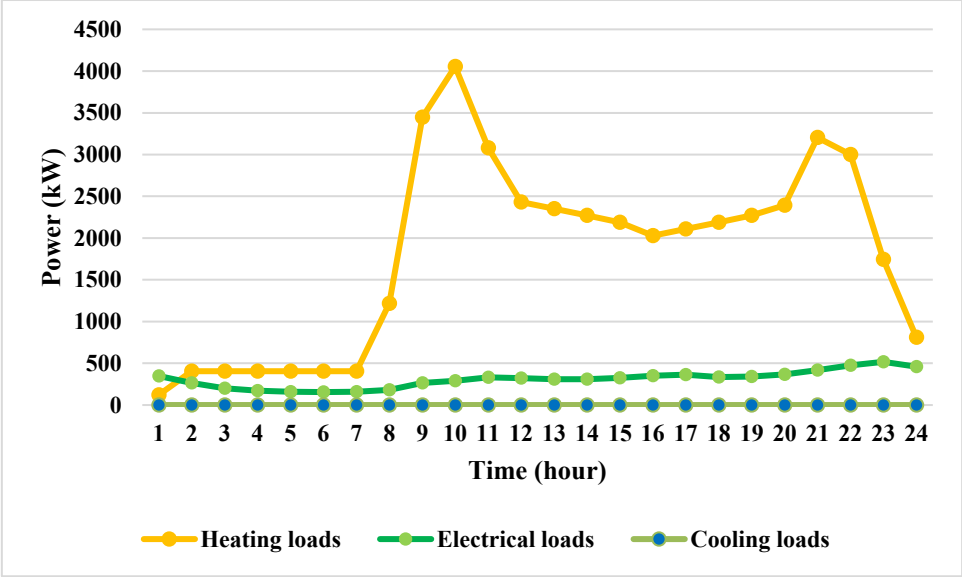

Figure 5. The various loads of SEH

Case studies: Results and Discussion

To evaluate the proposed model and investigate the system under different scenarios, we define two different case studies as follows:

- *Case study I*: The SEH is operated under a day-ahead optimization framework using a multi-objective formulation, without the integration of DRPs.
- *Case study II*: as the main case study, we explore the optimization of SEH with the implementation of both thermal and electrical DRPs with a multi-objective structure.

The study examines an eco-environmental trade-off solution obtained for w_1=0.5, w_2 =0.5

Case study I. As shown in **Table 4**, SEH operates without implementing electrical and thermal DRPs. The operating cost and total CO_2 emissions are 1436 EUR and 11732 kg, respectively. Additionally, the decision-maker purchased 391 kWh of electricity from the upstream grid over the 24 hours.

Table 4. The optimization results of SEH without DRP

	Operation Cost [EUR]	CO_2 [kg]	Total electric energy from the grid [kWh]
SEH	1436	11732	391

For each hour, the upstream grid and the SEH operator exchange net electrical power as depicted in **Figure 6**. Positive numbers mean that power is being imported (bought), while negative numbers mean that power is being exported (sold) to the grid. This is because of price signals and the need of grid power to satisfy the electric energy balance. Between 05:00 and 10:00, there is a significant net export phase, with the highest export level of approximately 270 kW at 07:00. This aligns with the morning price spike, which enables the SEH to profit from additional electricity generated by CHP units operating at full capacity to meet winter heating needs. The profile changes to net import from 11:00 to 13:00. This is precisely in correspondence with lowest grid power price (8.92 cEUR/kWh at 12:00). The optimization algorithm buys cheap power from the grid during this time to make up for shortfalls and charge internal storage assets (batteries), which keeps internal generation from being too expensive. The hub has almost no or slightly negative (export) interaction with the grid during the critical evening price peak (18:00-20:00). This shows that internal flexibility works to keep the hub from the highest costs (16.16 cEUR/kWh), which is the goal of peak load shaving and reducing the need for expensive evening grid imports.

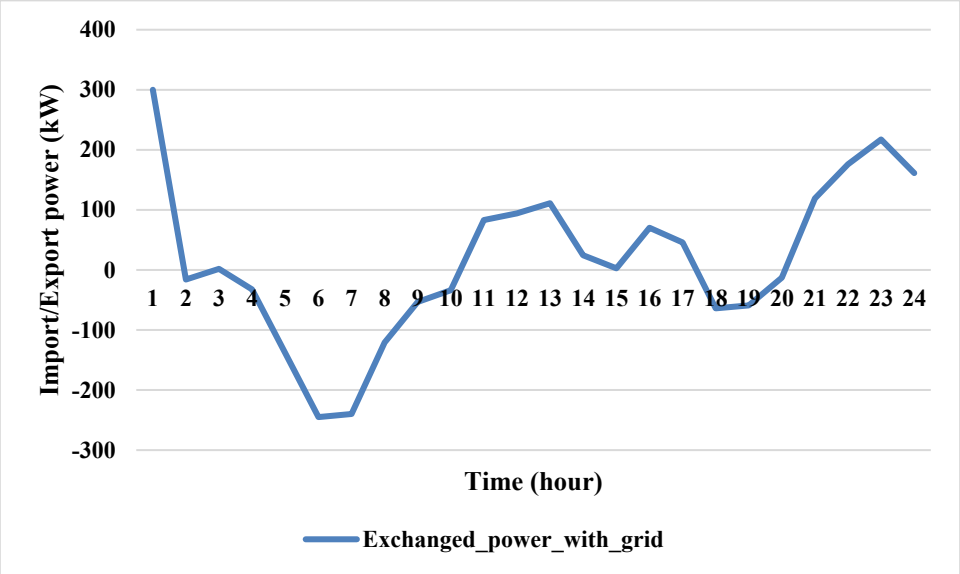

Figure 6. The exchanged electrical power between SEH and the grid without DRP

The performance of electrical storage system, as another key element of the system, is evaluated in **Figure 7**. It is evident that the optimization algorithm is implemented effectively, such that the electrical storage system performance tracks electricity price fluctuations. Storage is charged at hours with lowest electricity price, for example, between 3 – 5 AM and 12 – 4 PM, to achieve the most feasible charging. In contrast, during peak-price hours, storage is used to reduce operating costs and is discharged during high-price hours. This operation strategy consisting of using the battery to improve SEH's economic efficiency by shifting energy use away from costly peak periods represents an optimal strategy.

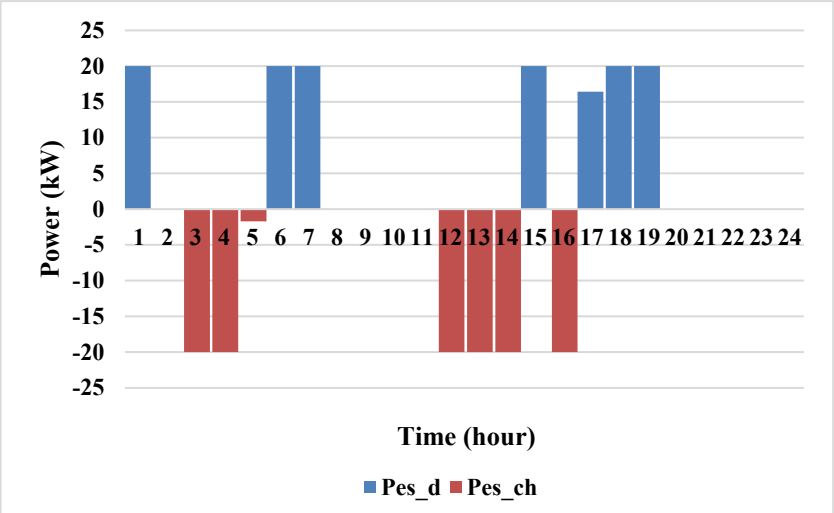

Figure 7. The electrical storage operation without DRP

Case study II. In this case study, we examine the SEH optimization with integrated DRP. As shown in **Table 5**, implementing DRP across both the thermal and electrical sections reduced the total optimization cost of SEH by 3% to 1391 EUR, while total CO_2 emissions remained unchanged. By shifting loads from expensive hours to cheaper periods, the SEH operator gained economic benefits through SEH operations optimization.

Table 5. The comparative analysis of optimization results with/without DRP

	Total operation cost [EUR]	Total CO_2 emissions [kg]
SEH	1436	11732
SEH_DRP	1391	11734
Improvement (%)	3	≈ 0

As **Figure 8** clearly shows, the DRP plays an indispensable role in SEH optimization. With DRP, the decision-maker imported a total of 364 kWh from the grid throughout the day, whereas without DRP it imported 391 kWh. DRP significantly reduces reliance on the grid and reduces demand stress on the electrical network. During off-peak hours, such as 10–14 AM, more grid power is bought, and during peak-price hours, the excess power is sold back to the grid. By implementing integrated DRPs, the SEH gains the necessary capacity headroom and frees up internal resources. This flexibility enables SEH to significantly increase its midday imports during the price valley (low prices) and to make higher-volume exports during the morning and evening peaks. This strategy minimizes total costs by increasing bidirectional power flow and shifting rigid baseline operation to a volatile, profit-driven trading profile.

Although the absolute reduction in grid imports is 27 kWh, this signifies a 7% improvement in SEH's energy self-sufficiency. This reduction is strategically achieved by shifting loads during critical peak-price windows, thereby reducing stress on the upstream network without violating user comfort constraints.

It is observed that implementing the DRP significantly reduces operational costs; however, total CO_2 emissions remain nearly unchanged (11,732 kg vs. 11,734 kg). This outcome is primarily attributed to the residential cluster's heat-led operation during the examined winter period. Due to the high thermal demand, the gas-fired boiler and combined heat and power (CHP) units must operate at high capacities to ensure adequate heat supply. The DRP mainly shifts electrical loads to lower-price periods, thereby enabling economic arbitrage. However, it does not reduce the underlying thermal demand nor substitute the natural gas required for thermal demand. Consequently, the overall emissions profile remains largely unaffected. Achieving substantial emission reductions during winter operation would require structural changes to the energy supply mix, such as greater integration of renewable thermal sources. Such measures would help decouple thermal comfort from fossil fuel combustion and enable meaningful reductions in CO_2 emissions.

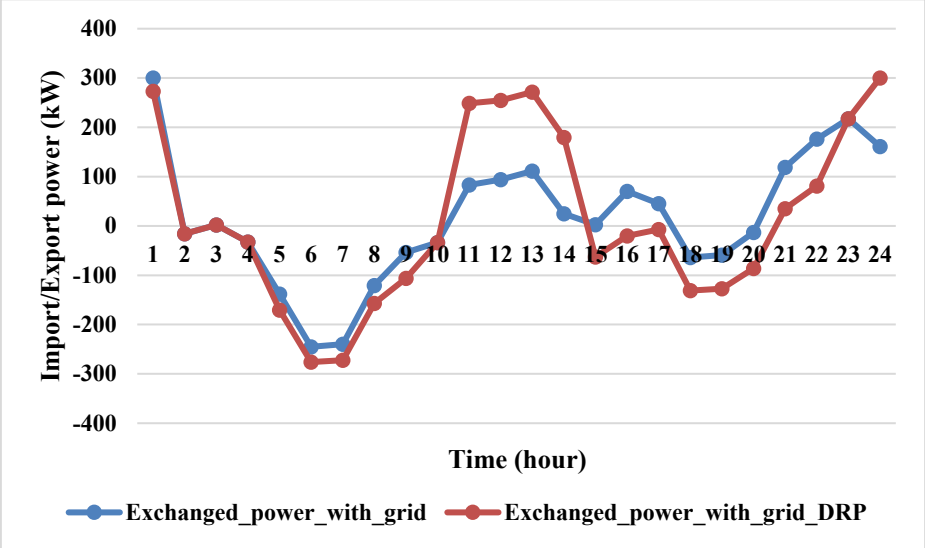

Figure 8. The comparison of exchanged power between SEH and the grid with/without DRP

Figure 9 shows that the CHP serves as the primary internal baseload supplier, whereas the grid imports (Pg, light green) cover only the supply-demand deficit during off-peak price hours. The decision maker employs three distinct layers of flexibility to manage volatility: DRP is actively used throughout the day to modulate the baseline load via shifting (DRP_up/DRP_down). The electrical storage executes fast arbitrage cycles (charging at noon, discharging during peaks), whereas the hydrogen system provides long-duration capacity, with the electrolyzer consuming power during the mid-day price valley and the fuel cell contributing supply during the evening peak. This cascading dispatch of resources ensures that the users' demands are met with high reliability and maximum economic efficiency.

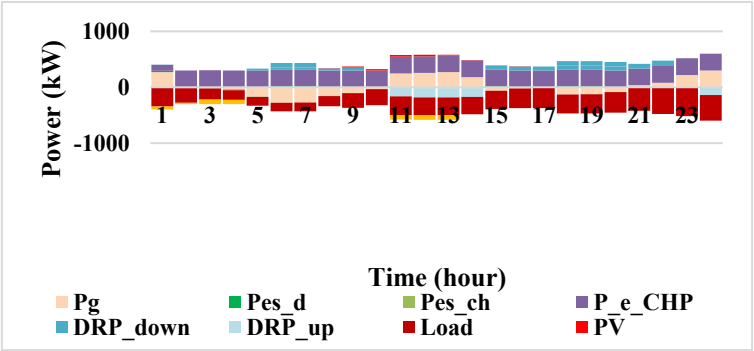

Figure 9. The electrical balance of SEH with DRP

Figure 10 reveals a profoundly heat-led operation for SEH day-ahead optimization. The bar chart shows that this residential cluster has a considerably higher heating load than its electrical load. The boiler is the largest single-generation asset throughout the day, supported by CHP operating at its maximum load. The central heating load represents the primary demand and fluctuates significantly, peaking during the day (e.g., hours 9 – 11) and in the evening (e.g., hours 20 – 22).

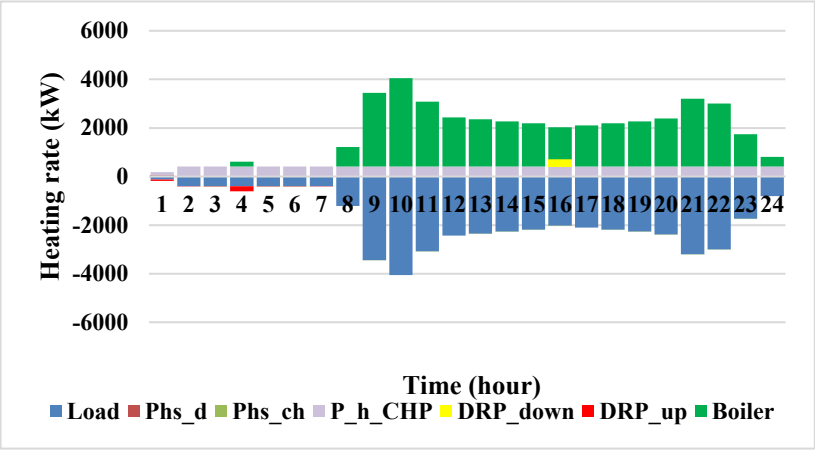

Figure 10. The thermal balance of SEH with DRP

Although the gas-fired boiler provides most of the heat in **Figure 10** to cover winter demand, the hydrogen system still plays a crucial role in keeping the hub electrically flexible. By charging around midday and discharging during the evening peak, the P2H2P loop allows the SEH to separate the electricity it buys from how it must operate its thermal units. In this way, the SEH behaves differently from a conventional district heating plant, actively using hydrogen to exploit price fluctuations in the electricity market and lower overall operating costs.

Figure 11 shows that DRP operates as a virtual battery, shifting electrical loads during off-peak periods to deliver economic value. The system shows a clear negative correlation between price and consumption, indicating that the load shifting effectively reduces operational costs. The most significant load shifting occurs between 10:00 and 14:00, when the price reaches its daily lowest value of 8.92 cEUR/kWh. This planned use of cheap energy keeps the cost of meeting the hub's total electrical demand as low as possible. On the other hand, consumers reduced their loads during peak-price hours such as 5:00 – 9:00 and 15:00 – 22:00. The E_DRP cuts demand during these expensive times, which reduces costs due to grid imports.

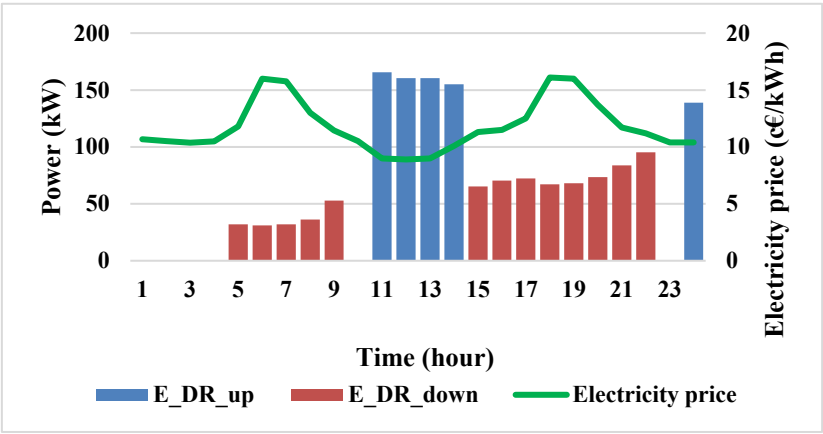

Figure 11. The DRP's performance during the day-ahead optimization

The performance of the hydrogen system, as depicted in **Figure 12**, clearly proves that it acts effectively as a long-duration storage asset. The electrolyzer produces hydrogen and consumes electricity during low-price hours between 1:00-4:00 AM and 11:00 – 01:00 PM, while the fuel cell converts hydrogen into power to assist the system in satisfying demand during peak-price hours, for example, from 6:00 – 8:00 PM. This highly price-responsive operation validates the economic viability of the hydrogen system in exploiting market volatility.

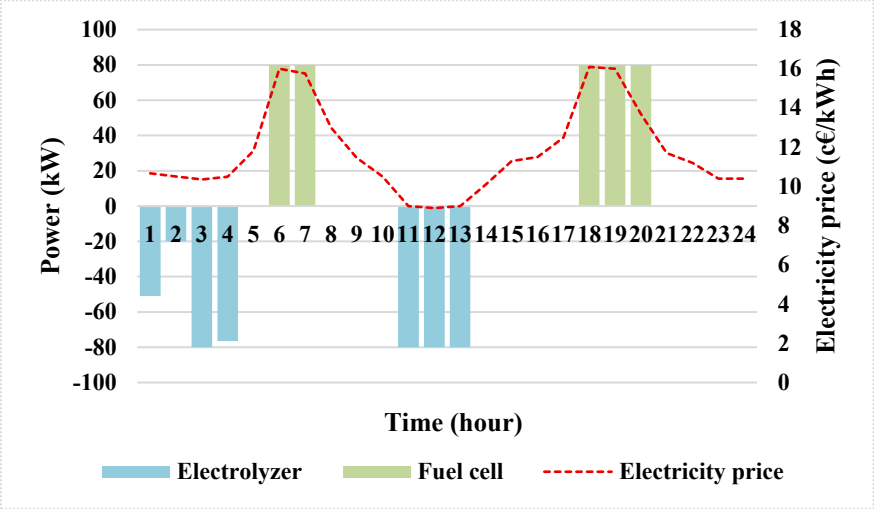

Figure 12. The hydrogen system performance for the day-ahead optimization

The P2H2P chain achieves a solid round-trip efficiency of 58.5%, based on the assumed electrolyzer efficiency of 90% and fuel cell efficiency of 65%. Even with the energy losses during conversion, the hydrogen system represents still a good financial option because it can take advantage of changing electricity prices: the difference between the low daytime price (8.92 cEUR/kWh) and the high evening price (16.16 cEUR/kWh) is enough to make up result, the hydrogen loop operates as a strategic flexibility asset, lowering total operating costs by 3% while strengthening the SEH's resilience to grid price fluctuations.

CONCLUSION

In this study, a smart energy hub (SEH) serving a residential building cluster was analysed for a winter-day operation in Torino, Italy. The SEH operation was first scheduled using a multi-objective optimization without integrated DRPs in Case Study 1, and then optimized in Case Study II with coordinated thermal and electrical DRPs. We found that, without DRP as a flexibility component, the decision-maker relied more on the grid when importing 391 kWh of electricity, whereas with DRP, only 364 kWh was taken from the grid. Additionally, simulation results indicated that other flexible equipment, including the hydrogen system and energy storage systems, were effectively utilized during the day. With DRPs, the total operating cost decreased by 3%, while emissions remained unchanged. The DRPs served as an economic amplifier, enabling the operator to execute high-volume energy arbitrage and generate higher profits by leveraging market volatility. Additionally, the hydrogen system improved SEH resilience by strategically performing charging/discharging cycles during different price periods. While the 3% reduction in operational costs represents a daily snapshot, these savings accumulate over the long-term project lifecycle. Although this study focuses on day-ahead operational scheduling, the results indicate that DRPs may act as economic amplifiers for capital-intensive assets such as hydrogen systems, thereby enhancing their economic viability in volatile markets.

The results indicated that highly granular demand-side management is necessary for capital-intensive assets such as hydrogen to realize their full economic potential. Future research should focus on integrating innovative bidding mechanisms and establishing robust optimization frameworks to ensure strong performance amid market price fluctuations and uncertainties in renewable generation. Moreover, future research should also integrate these operational findings into broader investment planning frameworks.

NOMENCLATURE

Symbols

$C_{\mathrm{H2}}^{\max}/C_{\mathrm{H2}}^{\min}$	maximum/minimum capacity of hydrogen storage	[kWh]
CI_{G}	carbon intensity of the grid	[kg/kWh]
CI_{gas}	carbon intensity of gas	[kg/kWh]
$COP_{\mathrm{ec}}, COP_{\mathrm{cs}}, COP_{\mathrm{ac}}$	performance coefficients of EC, CS, AC	[-]
CO_{curt}	coefficient of maximum curtailed load	[-]
$C_{\mathrm{ec}}^{t}, C_{\mathrm{ac}}^{t}, P_{\mathrm{csd}}^{t}$	cooling power of EC, AC, and CS	[kWh]
C_{H2}^{t}	stored hydrogen in hydrogen tank	[kWh]
$E_{\mathrm{es}}^{t}, E_{\mathrm{hs}}^{t}, E_{\mathrm{cs}}^{t}$	energy stored in ES, HS, CS	[kWh]
$E_{\mathrm{hs}}^{\min}/E_{\mathrm{hs}}^{\max}$	minimum/maximum capacities of HS	[kWh]
$E_{\mathrm{cs}}^{\min}/E_{\mathrm{cs}}^{\max}$	minimum/maximum capacities of CS	[kWh]
$E_{\mathrm{es}}^{\min}/E_{\mathrm{es}}^{\max}$	minimum/maximum capacities of ES	[kWh]
$H_{2}{}_{\mathrm{industry}}^{t}$	input hydrogen of hydrogen-based industries	[kWh]
G_{b}^{t}	imported gas from the network by boiler	[m^3/h]
G_{chp}^{t}	imported gas from the gas network by CHP units	[m^3/h]
$G_{\mathrm{b}}^{\max}$	maximum imported natural gas of boiler	[m^3/h]
$G_{\mathrm{chp}}^{\max}$	maximum imported gas of CHP	[m^3/h]
$I_{\mathrm{FC}}^{t}/I_{\mathrm{elz}}^{t}$	binary variables of fuel cell/electrolyzer	[-]
$I_{\mathrm{down}}^{\mathrm{h},t}/I_{\mathrm{up}}^{\mathrm{h},t}$	binary variable of down / up of heating DR	[-]
$I_{\mathrm{up}}^{\mathrm{e},t}/I_{\mathrm{down}}^{\mathrm{e},t}$	binary variable of down / up of electrical DR	[-]
$K_{\mathrm{c}}^{\mathrm{h},t}/K_{\mathrm{d}}^{\mathrm{h},t}$	binary variable for HS charging/discharging constraint	[-]
$K_{\mathrm{c}}^{\mathrm{c},t}/K_{\mathrm{d}}^{\mathrm{c},t}$	binary variable for CS charging/discharging constraint	[-]
$K_{\mathrm{c}}^{\mathrm{e},t}/K_{\mathrm{d}}^{\mathrm{e},t}$	binary variable of ES charging/discharging	[-]
LHV	lower heat value of natural gas	[kWh/m^3]
$MR_{\mathrm{up}}^{\mathrm{h}}/MR_{\mathrm{down}}^{\mathrm{h}}$	maximum coefficient for the up/down of the heating load	[kW]
$MR_{\mathrm{up}}^{\mathrm{e}}/MR_{\mathrm{down}}^{\mathrm{e}}$	maximum coefficient for up/down of load	[kW]
OM_{B}	maintenance cost coefficient of boiler	[cEUR/kWh]
OM_{CHP}	maintenance cost coefficient of CHP	[cEUR/kWh]
$P_{\mathrm{ec}}^{\max}, P_{\mathrm{cooling}}^{\max}$	maximum electricity input of EC/CS	[kW]
PEN_{curt}	penalty of load curtailment	[cEUR/kWh]
$P_{\mathrm{FC}}^{\max}/P_{\mathrm{FC}}^{\min}$	maximum/minimum output power of fuel cell	[kW]
$PH_{\mathrm{ac}}^{\max}$	maximum input heat of AC	[kW]
$P_{\mathrm{chp}}^{\max}$	maximum output power of CHP	[kW]
$P_{\mathrm{elz}}^{\max}/P_{\mathrm{elz}}^{\min}$	maximum/minimum input power of electrolyzer	[kW]
Ph_{b}^{t}	output heat power from boiler units	[kW]

$P^{\mathrm{hl},t}, P^{\mathrm{el},t}, CL^t$	heating, electrical, and cooling loads	[kW]
$P^t_{\mathrm{hs},c}/P^t_{\mathrm{hs,d}}$	charging/discharging heat rate of HS	[kW]
$PE^t_{\mathrm{chp}}, PH^t_{\mathrm{chp}}$	ouptput electrical and heat power from CHP	[kW]
P^t_{FC}	output power of fuel cell	[kW]
PH^t_{ac}	imported heat rate to AC	[kW]
$P^t_{\mathrm{cs,c}}$	cooling charging rate of CS	[kW]
$P^{\mathrm{e},t}_{\mathrm{curt}}$	curtailed load	[kW]
$P^{\mathrm{h},t}_{\mathrm{down}}/P^{\mathrm{h},t}_{\mathrm{up}}$	shift up/down of heat load by DRP	[kW]
P^t_{ec}	imported power to EC	[kW]
P^t_{elz}	Imported power to electrolyzer	[kW]
$P^t_{\mathrm{es,c}}/P^t_{\mathrm{es,d}}$	charging/discharging power of ES	[kW]
P^t_{g}	imported power from the primary grid	[kW]
$P^{\mathrm{e},t}_{\mathrm{up}}/P^{\mathrm{e},t}_{\mathrm{down}}$	shift up/down of electrical load by DRP	[kW]
Δt	hourly time slot	[1 hour]

Greek letters

Y_t	electricity price	(cEUR/kWh)
$\delta_{\mathrm{es}}, \delta_{\mathrm{cs}}, \delta_{\mathrm{hs}}$	loss coefficient of energy storage systems	[%]
$\eta_{\mathrm{hs,c}}/\eta_{\mathrm{hs,d}}$	charging/discharging efficiency of HS	[%]
η_{B}	efficiency of a gas-fired boiler	[%]
$\eta^{\mathrm{h}}_{\mathrm{chp}}, \eta^{\mathrm{e}}_{\mathrm{chp}}$	CHP thermal and electrical efficiency	[%]
$\eta_{\mathrm{cs,c}}/\eta_{\mathrm{cs,d}}$	charging/discharging efficiency of CS	[%]
$\eta^{\mathrm{elz}}/\eta^{\mathrm{FC}}$	electrolyzer/fuel cell efficiency	[%]
$\eta_{\mathrm{es,c}}/\eta_{\mathrm{es,d}}$	charging/discharging efficiency of ES	[%]
λ_t	gas price	(cEUR/m^3)

Subscripts and superscripts

t	index of time

Abbreviations

AC	Absorption Chiller
CHP	Combined Heat and Power
CS	Cooling Storage
DRP	Demand Response Program
EC	Electrical Chiller
ES	Electrical Storage
H_2	Hydrogen
HS	Heating Storage
MILP	Mixed Integer Linear Programming
P2H2P	Power-To-Hydrogen-To-Power
SEH	Smart Energy Hubs
VRE	Variable Renewable Energy

REFERENCES

1. Liu, Q., Li, W., Zhao, Z. and Jian, G., Optimal operation of coordinated multi-carrier energy hubs for integrated electricity and gas networks, *Energy*, Vol. 288, 2024, https://doi.org/10.1016/j.energy.2023.129800.
2. Barati, A., Karimi, H. and Jadid, S., Multi-objective operation of interconnected multi-energy systems considering power to gas and gas to power systems, *International*

Journal of Electrical Power and Energy Systems, Vol. 158, 2024, https://doi.org/10.1016/j.ijepes.2024.109986.

3. Jodeiri-Seyedian, S. S., Fakour, A., Nourollahi, R., Zare, K. and Mohammadi-Ivatloo, B., Eco-environmental impacts of x-to-x energy conversion on interconnected multi-energy microgrids: A multi-objective optimization, *Sustainable Cities and Society*, Vol. 99, 2023, https://doi.org/10.1016/j.scs.2023.104947.
4. Heikal, A. M. A., Aleem, S. H. E. A., El-Sehiemy, R. A. and Abdelaziz, A. Y., Robust techno-economic optimization of energy hubs under uncertainty using active learning with artificial neural networks, *Scientific Reports*, Vol. 15, No. 1, 2025, https://doi.org/10.1038/s41598-025-12358-z.
5. Mei, J. and Ahmad, W., Optimizing energy management in integrated natural gas and electricity networks: A smart energy hub approach using cloud-based DSM and game-theoretic optimization, *Computers and Industrial Engineering*, Vol. 210, 2025, https://doi.org/10.1016/j.cie.2025.111535.
6. Giehl, J., Hentschel, D., Ciprian, L. and Weibezahn, J., Fueling the future: Optimizing Power-to-X production in renewable energy hubs through flexible operating units, *Energy*, Vol. 333, 2025, https://doi.org/10.1016/j.energy.2025.137211.
7. Wang, F., Zheng, W., Zhao, J. and Forghan, H., Enhancing efficiency and reliability of multi-energy systems: A hybrid heuristic algorithm for interconnected energy hubs, *Electric Power Systems Research*, Vol. 231, 2024, https://doi.org/10.1016/j.epsr.2024.110273.
8. Garg, A., Niazi, K. R., Tiwari, S., Sharma, S. and Rawat, T., Optimal energy management of multi-carrier energy system considering uncertainty in renewable generation, *Scientific Reports*, Vol. 15, No. 1, 2025, https://doi.org/10.1038/s41598-025-10404-4.
9. Ma, S., Mi, Y., Li, S., Wang, X., Li, D. and Wang, P., Bi-level operation model for energy hub based on energy-carbon coordination optimization framework, *Energy*, Vol. 333, 2025, https://doi.org/10.1016/j.energy.2025.137449.
10. Wang, D. and Ying, C., Optimizing performance and economic viability of combined energy systems: A novel energy hub framework, *Alexandria Engineering Journal*, Vol. 124, pp 188–203, 2025, https://doi.org/10.1016/j.aej.2025.03.105.
11. Moazen, M. and Saghafi, M., Performance optimization of an energy hub in the presence of a micro modular reactor and renewable energy sources, *Nuclear Engineering and Design*, Vol. 444, 2025, https://doi.org/10.1016/j.nucengdes.2025.114426.
12. Yan, L., Lyu, L. and Niu, Q., Towards efficient energy hubs: Two-stage robust optimization with compressed air storage, electric vehicles and renewable energy integration, *Journal of Energy Storage*, Vol. 111, 2025, https://doi.org/10.1016/j.est.2025.115338.
13. Wang, G., Pan, C., Wu, W., Fang, J., Hou, X. and Liu, W., Multi-time scale optimization study of integrated energy system considering dynamic energy hub and dual demand response, *Sustainable Energy, Grids and Networks*, Vol. 38, 2024, https://doi.org/10.1016/j.segan.2024.101286.
14. Yan, L., Deng, X. and Li, J., Integrated energy hub optimization in microgrids: Uncertainty-aware modeling and efficient operation, *Energy*, Vol. 291, 2024, https://doi.org/10.1016/j.energy.2024.130391.
15. Akbarizadeh, M., Niknam, T., Dehghani, M., Pourbehzadi, M., Javidi, G. and Sheybani, E., Multi-objective strategic offering of networked energy hubs in the day-ahead energy market according to uncertainty modelling, *Energy*, Vol. 314, 2025, https://doi.org/10.1016/j.energy.2024.134288.
16. Alghamdi, A. S., Alanazi, M., Alanazi, A., Qasaymeh, Y., Zubair, M., Awan, A. B. and Ashiq, M. G. B., Stochastic programming for hub energy management considering uncertainty using two-point estimate method and optimization algorithm, *CMES* -

Computer Modeling in Engineering and Sciences, Vol. 137, No. 3, pp 2163–2192, 2023, https://doi.org/10.32604/cmes.2023.029453.

17. Qian, J., Guo, Y., Wu, D., Liu, A., Han, Z., Liu, Z., Zhang, S. and Yang, X., Research on multi-time scale optimization of integrated energy system based on multiple energy storage, *Journal of Energy Storage*, Vol. 102, 2024, https://doi.org/10.1016/j.est.2024.113892.
18. Agabalaye-Rahvar, M., Mansour-Saatloo, A., Mirzaei, M. A., Mohammadi-Ivatloo, B. and Zare, K., Economic-environmental stochastic scheduling for hydrogen storage-based smart energy hub coordinated with integrated demand response program, *International Journal of Energy Research*, Vol. 45, No. 14, pp 20232–20257, 2021, https://doi.org/10.1002/er.7108.
19. Nasir, M., Rezaee Jordehi, A., Matin, S. A. A., Tabar, V. S., Tostado-Véliz, M. and Mansouri, S. A., Optimal operation of energy hubs including parking lots for hydrogen vehicles and responsive demands, *Journal of Energy Storage*, Vol. 50, 2022, https://doi.org/10.1016/j.est.2022.104630.
20. Darvishi, A., Ranjbar, B., Gharibi, R., Khalili, R. and Dashti, R., Multi-objective optimization of a socio-economic energy hub with demand response program and considering customer satisfaction, *Journal of Energy Storage*, Vol. 100, 2024, https://doi.org/10.1016/j.est.2024.113624.
21. Fan, L., Ji, D., Lin, G., Lin, P. and Liu, L., Information gap-based multi-objective optimization of a virtual energy hub plant considering a developed demand response model, *Energy*, Vol. 276, 2023, https://doi.org/10.1016/j.energy.2023.127462.
22. Gulraiz, A., Al Bastaki, A. J., Magamal, K., Subhi, M., Hammad, A., Allanjawi, A., Zaidi, S. H., Khalid, H. M., Hussain, A. I. G. A. and Said, Z., Energy advancements and integration strategies in hydrogen and battery storage for renewable energy systems, *iScience*, 2025, https://doi.org/10.1016/j.isci.2025.111945.
23. Abbas, T., Chen, S., Zhang, X. and Wang, Z., Coordinated optimization of hydrogen-integrated energy hubs with demand response-enabled energy sharing, *Processes*, Vol. 12, No. 7, 2024, https://doi.org/10.3390/pr12071338.
24. Zhu, G., Ye, M., Yu, X., Liu, J., Wang, M., Luo, Z., Liang, H. and Zhong, Y., Optimizing route planning via the weighted sum method and multi-criteria decision-making, *Mathematics*, Vol. 13, No. 11, 2025, https://doi.org/10.3390/math13111704.
25. Grodzevich, O. and Romanko, O., Normalization and other topics in multi-objective optimization, in *Proc. Fields–MITACS Industrial Problems Workshop*, Fields Institute for Research in Mathematical Sciences / MITACS, 2006.
26. JRC Photovoltaic Geographical Information System (PVGIS) - European Commission, https://re.jrc.ec.europa.eu/pvg_tools/en/, [Accessed: Sep. 11, 2025].
27. ENTSO-E, Transparency Platform, https://newtransparency.entsoe.eu/market/energyPrices, [Accessed: Oct. 29, 2025].
28. Yan, B., Di Somma, M., Luh, P. B. and Graditi, G., Operation optimization of multiple distributed energy systems in an energy community, in *Proceedings of the 2018 IEEE International Conference on Environment and Electrical Engineering and 2018 IEEE Industrial and Commercial Power Systems Europe (EEEIC/I&CPS Europe)*, pp 1–6, 2018, IEEE, https://doi.org/10.1109/EEEIC.2018.8494476.
29. Di Somma, M., Yan, B., Bianco, N., Graditi, G., Luh, P. B., Mongibello, L. and Naso, V., Design optimization of a distributed energy system through cost and exergy assessments, *Energy Procedia*, Vol. 105, pp 2451–2459, 2017, https://doi.org/10.1016/j.egypro.2017.03.706.

Paper submitted: 12.12.2025
Paper revised: 02.03.2026
Paper accepted: 04.03.2026